HARD PHOTONS FROM HEAVY-ION COLLISIONS[1]

K. NIITA, A.L. DE PAOLI, W. BAUER, T.S. BIRO, W. CASSING,
U. MOSEL

Institut für Theoretische Physik, Universität Giessen
6300 Giessen, West Germany

The production of high energy γ-rays in intermediate
energy nucleus-nucleus collisions is studied microscopically
within two different approaches. First we calculate energetic
photons as emerging from collective bremsstrahlung within TDHF
as well as Extended TDHF. It is found, however, that the double
differential spectra disagree with experimental data, both in
magnitude and angular distribution. In a second step we assume
high energy γ-rays to be produced by incoherent nucleon-nucleon
collisions. For this purpose we evaluate covariantly the photon
production from proton-neutron collisions in a vector (ω) and
scalar meson (σ) exchange model with coupling constants given
by the M2Y G-matrix in the nonrelativistic limit. We further-
more follow the proton-neutron collisional history by means of
a phase-space simulation based on the Vlasov-Uehling-Uhlenbeck
approach for proton-nucleus and nucleus-nucleus collisions
adding up incoherently the yields from each individual colli-
sion. The satisfactory agreement we obtain in comparison with
experimental data allows to conclude that energetic photons
dominantly arise from proton-neutron bremsstrahlung during the
early stage of the collision. Similar statements are found to
hold also for subthreshold pion production by independent
nucleon-nucleon collisions.

1. INTRODUCTION

High energy photon emission in heavy-ion collisions has
recently gained interest since it provides an additional probe for
the heavy-ion dynamics apart from energetic light particles or
pions[1-8]. A variety of models have been developed in the last years
ranging from collective bremsstrahlung[9-11] to 'statistical treat-
ments' of the A-body problem[12]. Emission from a hot spot and
production by nucleon-nucleon bremsstrahlung have been considered
as well[13-15]. Most of these approaches, however, lack a more
microscopic foundation on the underlying heavy-ion dynamics and
their range of validity should be determined by parameter-free
calculations. In this contribution we aim at solving the latter
problem with respect to collective bremsstrahlung as well as for
photon radiation from individual nucleon-nucleon collisions.

In Section 2 we outline the general framework and evaluate the double differential photon cross-section for $^{16}O+^{16}O$ at 80 MeV/u with TDHF as well as within the extended TDHF approach of Tohyama[16] which keeps track of the effect of residual nucleon-nucleon collisions on the collective current. A comparison with experimental data from Ref. [1] is included.

Nucleon-nucleon bremsstrahlung is an alternative production mechanism[13]. Indeed it was found in the calculations of Ko et al.[14] that neutron-proton bremsstrahlung was more important than coherent bremsstrahlung except for collisions of very heavy nuclei. Furthermore, neutron-proton (np) bremsstrahlung as evaluated for first chance np collisions within a quantum mechanical phase-space model[15] gives overall agreement with the total cross-section of photons above 50 MeV. In the case of exclusive measurements the double differential cross-sections can also be well understood within this approach[7].

However, the use of the soft photon limit[18] or the 1/ω expansion for the photon cross section in Refs.[13-17] might not be adequate[19]. We thus improve this description in Section 3 by evaluating in a covariant way the radiative corrections to the nucleon-nucleon vertices involving vector meson (ω) and scalar meson (σ) exchange in close analogy to studies performed in the later sixties[20] and early seventies[21,22]. We restrict ourselves to proton-neutron vertices since proton-proton bremsstrahlung was found experimentally to be more than an order of magnitude smaller than pn → pnγ[23].

We follow the nucleon-nucleon collisional history in time by means of numerical simulations based on the Vlasov-Uehling-Uhlenbeck equation[24-26] and evaluate perturbatively the photon yield from each individual collision (Section 4). A comparison of the calculated spectra with experimental data for proton- and heavy-ion induced reactions is given in Section 5 which also includes scaling laws with respect to the mass of the colliding nuclei. A detailed analysis of initial and final phase-space distributions for $^{12}C+^{12}C$ and $^{12}C+^{40}Ca$ at 40 MeV/u is performed in Section 6 while in Section 7 the present approach is applied to subthreshold pion production.

2.GENERAL FORMULATION OF PHOTON PRODUCTION BY RADIATING CHARGES

We consider the interaction density

$$H^{int} = j_\mu A^\mu \tag{2.1}$$

between the nuclear electromagnetic current j^μ and the electro-magnetic field A^μ within Heaviside-Lorentz units. The S-matrix for this Hamiltonian density is given in first order perturbation theory by

$$S = 1 - i \int d^4x \ j_\mu A^\mu \tag{2.2}$$

where the operators are described in the interaction picture. The number of photons in the interval $[k,k+\Delta k]$ is given by

$$\frac{dn}{dk^3} = \sum_\lambda \sum_f | \int \langle \hat{k},\lambda | | \langle \Psi^f | j_\mu A^\mu | \Psi^i \rangle | | 0 \rangle \ d^4x |^2 \tag{2.3}$$

where Ψ^i and Ψ^f denote the initial and final states of the nuclear system while $||0\rangle$ denotes a zero-photon state and $||\hat{k},\lambda\rangle$ a single photon state with photon 4-vector $\hat{k}$ and polarization λ. The restriction to single photon states in (2.3) should be justified in the intermediate energy domain from roughly 20 MeV/u to 160 MeV/u because the coupling constant of the electromagnetic interaction is small.

In the radiation gauge eq. (2.3) may be written in the form

$$\frac{dn}{dk^3} = \frac{1}{2\omega} \sum_f \sum_\lambda (2\pi)^{-3} | \int d^4x \ e^{ikx} \langle \Psi^f | j \cdot \epsilon(\hat{k},\lambda) | \Psi^i \rangle |^2 \tag{2.4}$$

where $\epsilon(\hat{k},\lambda)$ is a unit polarization vector corresponding to a photon with $(\hat{k},\lambda)$. The two polarization vectors $\epsilon(\hat{k},\lambda_1)$ and $\epsilon(\hat{k},\lambda_2)$ are orthogonal to $k/|k|$, which implies that photons only probe the transverse component of the nuclear current.

2.1 TDHF formalism

Neglecting all correlations between nucleons in eq. (2.4) except those induced by the mean field and the Pauli principle, we may replace the states Ψ^i and Ψ^f in (2.4) by Slater determinants. We determine the time dependence of these Slater determinants by means of the TDHF method. In this way we retain the collective stopping of the two nuclei by the mean-field and treat the important energy-momentum correlation in the single-particle (s.p.) states. Furthermore, we include dynamical distortions both in x- and in p-space and treat the Pauli principle exactly. In addition to the s.p. limit for the states Ψ^i and Ψ^j we restrict to the s.p. limit of the current which in the nonrelativistic limit is given by[27]

$$\mathbf{j}_q = -\frac{ie}{2m}(1-\tau_3)(\varphi^+\nabla\varphi - \varphi\nabla\varphi^+) + \mu_q\nabla \times (\varphi^+\sigma\varphi), \qquad (2.5)$$

where φ is a nucleon field operator. The first part represents the 'Schrödinger'-convection current and the second part the spin current. The magnetic moments are given by

$$\mu_p = 2.79 \ \mu_k = 2.79\frac{e}{2m} \ , \qquad \mu_n = -1.91 \ \mu_k \ . \qquad (2.6)$$

The final expression for the matrix elements of the current operator in eq. (2.4) is

$$\mathbf{j}^p_{ij} = -\frac{ie}{2m}(\varphi_{jp}\nabla\varphi_{ip} - \varphi_{ip}\nabla\varphi_{jp}) + \mu_p\nabla \times (\varphi_{jp}\sigma\ \varphi_{ip}) \qquad (2.7)$$

for protons and

$$\mathbf{j}^n_{ij} = \mu_n\nabla \times (\varphi_{jn}\ \sigma\ \varphi_{in}) \qquad (2.8)$$

for neutrons where $\varphi(\mathbf{r};t)$ are time-dependent s.p. states building up the Slater determinants Ψ^i and Ψ^f in (2.4). From eq. (2.8) we see that neutrons have a nonvanishing contribution to the photon yield which is important at higher photon energies[28]. The number of photons in the interval $[\mathbf{k},\mathbf{k}+\Delta\mathbf{k}]$ is then given by

$$\frac{dn}{dk^3} = \frac{(2\pi)^{-3}}{2\omega} \sum_\lambda |\ \sum_h \int d^4x \ e^{i\hat{k}x} \ \mathbf{j}_{hh}\cdot\boldsymbol{\epsilon}\ (\hat{\mathbf{k}},\lambda)|^2$$
$$+ \frac{(2\pi)^{-3}}{2\omega} \sum_\lambda \sum_{p,h} |\int d^4x \ e^{i\hat{k}x} \ \mathbf{j}_{ph}\cdot\boldsymbol{\epsilon}(\hat{\mathbf{k}},\lambda)|^2 \ , \qquad (2.9)$$

where the sums over p and h run over particle- and hole-states, respectively.

The first part of eq. (2.9) describes the photon production via the space and time variation of the one-body current (collective bremsstrahlung); the second part gives in addition the yield due to electromagnetic transitions between occupied and unoccupied time-dependent s.p. states during the collective deceleration.

The total yield of photons per solid angle $d\Omega$ in the interval $(\omega,\omega+\Delta\omega)$ is finally given by an integral over impact parameter b using $d^3k = \omega^2 d\omega d\Omega$, because the s.p. states φ also depend on the impact parameter b of the nucleus-nucleus collision, i.e.

$$\frac{d^2\sigma}{d\omega d\Omega} = \omega^2 \int_0^\infty \frac{dn(\mathbf{b})}{dk^3} \ d^2b \ . \qquad (2.10)$$

Apart from the solution of the time-dependent Hartree-Fock problem for fixed b with respect to occupied and unoccupied s.p. states, the evaluation of eq. (2.9) requires a four dimensional Fourier integration for a large number of different Slater-determinants. Some approximations, which do not effect the final conclusions, thus appear appropriate.

We replace the integral over impact parameter in eq. (2.10) by the double differential photon multiplicity $dn(\bar{b})/dk^3$ at an average impact parameter $\bar{b}$ and multiply by the geometrical cross section, i.e.

$$\frac{d^2\sigma}{d\omega d\Omega} = \omega^2 \frac{dn(\bar{b})}{dk^3} \times \pi\, r_0^2\, A^{2/3} \, , \qquad\qquad (2.11)$$

where A denotes the mass-number of the target or projectile in case of symmetric collisions. The radius parameter r_0 in (2.11) is assumed to be $r_0 \approx 1.2$ fm. This approximation separates the more trivial geometrical aspects of heavy-ion collisions at high energy from the elementary production mechanism invoked in eq. (2.9). We concentrate on the system $^{16}O+^{16}O$ at 80 MeV/u laboratory energy and adopt $\bar{b} = 1.5$ fm as an average impact parameter. The evaluation of (2.9) is straight forward once the time dependent Slater determinants have been produced by a TDHF calculation[29].

A problem arises with respect to the Fourier transformation in time which induces a numerical uncertainty due to the finite time interval considered. Averaging over initial and final time intervals we obtain a reasonable estimate of the τ-cross section $d^2\sigma/dEd\Omega$, which is displayed in Fig. 1 for collective bremsstrahlung, i.e. the first part of (2.9), in terms of the full lines at 5°, 45° and 85° in the reaction plane with respect to the beam axis. Though only three angles are considered (in the nucleus-nucleus center-of-mass system), the results indicate a dominant quadrupole-type distribution as expected from the interference pattern of two decelerated equal charge distributions[18]. The numerical uncertainty due to the finiteness of the time-interval is displayed in terms of the vertical lines for the photon yield at 45° and is of the same order of magnitude for the other angles.

2.2 Comparison with experiment

How do these results compare with experiment? First of all, experimental angular distributions turn out to be rather flat in the nucleon center of mass system in contrast to a quadrupole distribution for collective bremsstrahlung[18]. In addition, the experimental photon yield (full dots in Fig. 1) for $^{12}C+^{12}C$ at 84 MeV/u and 90°, a system which should be roughly comparable to the present calculation, is at least about an order of magnitude larger. Furthermore, the inverse slope of the calculated spectrum is significantly smaller than that of the data.
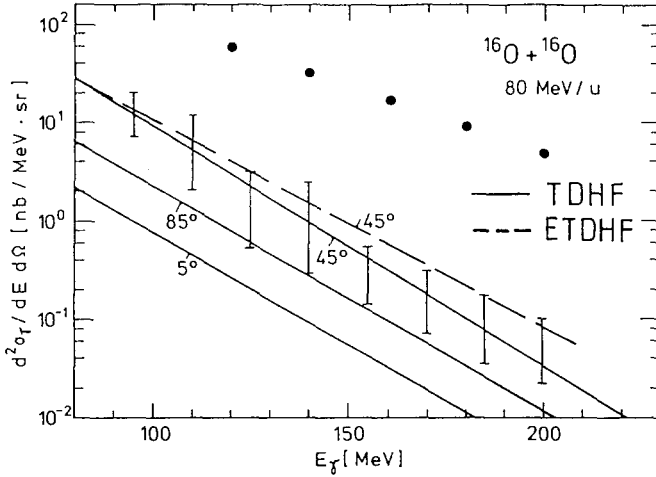
Fig. 1: The double differential photon cross section for $^{16}O+^{16}O$ at 80 MeV/u as resulting from collective bremsstrahlung (full lines) at $\theta = 5^{\circ}$, 45° and 85° in the center-of-mass system. The numerical uncertainty is indicated by the vertical error bars at 45°. The dashed line represents the corresponding result of the collective bremsstrahlung at 45°, in which effects from residual nucleon-nucleon collisions on the nuclear current are taken into account. The experimental data (full dots) are taken from Ref.[1].

One might argue that the collective deceleration by the mean-field in the one-body limit a priori is expected to be too small at these bombarding energies since residual two-body collisions have been neglected. In order to study the effect of residual nucleon-nucleon interactions on the collective current, calculations have been performed within the extended TDHF approach of Tohyama[16] where the relaxation due to residual nucleon-nucleon collisions is treated explicitly. A very short relaxation time $\tau = 2.10^{-23}$ s was assumed in order to obtain an upper limit for effects of such a collision term. The evaluation of the Fourier transform of the current as well as the limits for the photon cross section are the same as before. The results are shown in Fig. 1 by the long dashed line ($\theta = 45^{\circ}$). Within the numerical accuracy achieved they do not indicate a significant enhancement of the photon yield due to collective bremsstrahlung.

The same order of magnitude is obtained for electromagnetic transitions between occupied and unoccupied time-dependent s.p. states, i.e. the second part of (2.9). Contrary to the collective bremsstrahlung contribution (cf. Fig. 1) the photon yield is

slightly enhanced at 90° in the center-of-mass system. The slope of the spectrum, furthermore, is flatter than that of the brems-strahlung contribution and close to that of the experimental data for $^{12}C+^{12}C$ at 84 MeV/u and 90° [28].

Summing up the contributions of collective bremsstrahlung (Fig. 1) and electromagnetic transitions for the higher γ-energies the minimum in the angular distribution at 90° disappears, but the sum accounts at most for 10 % of the measured cross section. Thus the experimentally observed photon yield in light systems cannot be attributed to collective bremsstrahlung or electromagnetic transitions between time-dependent states. In the next Section we therefore address the question of photon production by individual nucleon-nucleon collisions as an alternative source.

3. COVARIANT CALCULATION OF γ PRODUCTION IN PN COLLISIONS

According to experimental and theoretical studies the photon production in nucleon-nucleon reactions is dominated by the pn $\rightarrow$ pnγ process since pp $\rightarrow$ ppγ is suppressed by about an order of magnitude[23] due to destructive interference of the radiation from each of the two protons. Due to the rather involved 5-body kinematics in such reactions there are not enough experimental data to cover the complete range of γ-energies and -angles for all initial and final nucleon momenta. For the purpose of modeling γ-production in heavy-ion collisions we, therefore, cannot use the "free" pn $\rightarrow$ pnγ cross sections as "experimental" input.

Besides this "practical" problem there is a more physical motivation to use model calculations for describing the pn $\rightarrow$ pnγ process, namely that "free" elementary cross sections may be consi-derably different from in-medium cross sections[30]. In our earlier studies[15,17] we used the nonrelativistic long wavelength ($1/\omega$) expansion[18] for the elementary process pn $\longrightarrow$ pnγ, i.e.

$$\frac{d\sigma}{d\omega d\Omega_\gamma} = \frac{e^2}{4\pi} \frac{\pi R^2}{4\pi} \frac{\beta^2}{\omega} \left[\sin^2\theta_\gamma + \frac{2}{3} \right] \tag{3.1}$$

where β denotes the velocity of the nucleons in the nucleon-nucleon c.m. frame and πR^2 the angle integrated pn cross section.

In order to get rid of the $1/\omega$ expansion we use a fit for the in-medium nucleon-nucleon interaction in terms of two Yukawa potentials by Bertsch et al.[32] and consider a relativistic extension in terms of one-boson exchange of scalar- and vector-type with masses m_1 = 492.5 MeV = 1/0.4 fm^{-1}, m_2 = 788 MeV = 1/0.25 fm^{-1} and weight factors $g_1^2/4\pi$ = 4.356, $g_2^2/4\pi$ = 11.49, respectively. It

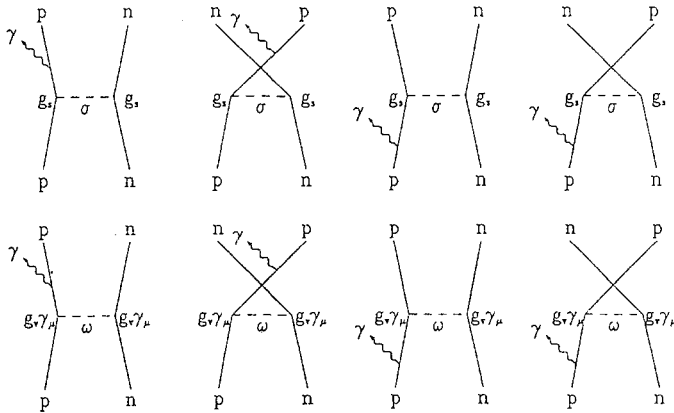**Fig. 2:** Feynman graphs corresponding to radiative corrections of scalar- and vector meson exchange in the process pn → pnγ.

is interesting to note that the masses of the exchanged mesons are surprisingly close to those used in the relativistic mean-field theory of nuclear structure[30].

For the transition matrix of the pn → pnγ process we have contributions from four different amplitudes according to photon radiation before or after the pn interaction and scalar or vector meson exchange. The antisymmetrization of the fermion final states brings an extra factor of 2, so altogether we deal with $8^2 = 64$ terms in the cross section formula (the corresponding amplitudes are depicted in Fig. 2 in terms of Feynman diagrams). For the detailed evaluation of the radiative corrections to the M2Y G-matrix we refer the reader to Ref.[36].

The resulting double differential photon cross section $d\sigma/d\omega d\Omega$ calculated with one-boson (scalar + vector) Feynman graphs and free nucleon masses (middle of Fig. 3) shows a characteristically flatter angular distribution than the "semi-classical" $1/\omega$-expansion (l.h.s. of Fig. 3), especially for high (near-threshold) photon energies in case of p+n at 200 MeV. Most of this flattening is due to a relativistic effect; even in the long wavelength approximation the dipole-bremsstrahlung is forward peaked[18]. By symmetrizing the cross section with respect to pn and np collisions we obtain an even flatter angular distribution (r.h.s. of Fig. 3).
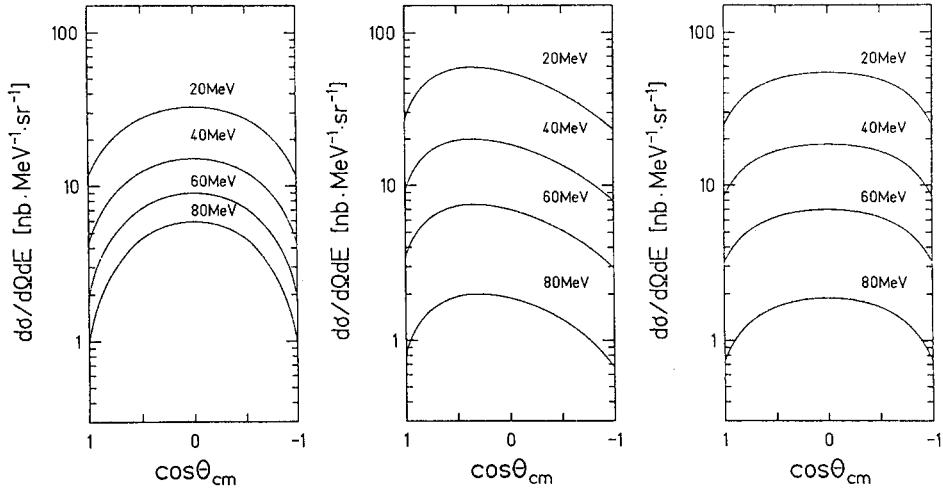
Fig. 3: Comparison of the double differential photon cross section from 200 MeV pn → pnγ in the semiclassical (1/ω) limit (l.h.s.) and the relativistic OBE approximation (middle) for the various photon energies indicated in the figure. The photon angular distribution for the relativistic OBE approach symmetrized with respect to pn and np collisions is shown in addition (r.h.s.).

4. HEAVY-ION REACTION DYNAMICS

After the evaluation of the elementary production cross section for high energy photons, we need a model for the heavy-ion reaction dynamics to obtain information on the number of pn collisions during the heavy-ion collision and the momentum distribution of protons and neutrons. In this context we used a phase-space distribution based on TDHF dynamics[15], but had to assume ad hoc that the photons were produced by first chance pn collisions only.

It is therefore desirable to use a transport theory for heavy-ion reactions which keeps track of the np collisional time-evolution. The only workable transport theory for heavy ion reactions in three dimensions at present is based on the Vlasov-Uehling-Uhlenbeck equation[24-26],

$$\partial/\partial t \; f_1 - \mathbf{v}_p f_1 \cdot \mathbf{v}_r U + \mathbf{v}_r f_1 \cdot \frac{\mathbf{P}}{m}$$

$$= \frac{4}{(2\pi)^3} \int d^3 p_2 \; d^3 p_3 \; d\Omega \; v_{12} \frac{d\sigma}{d\Omega} \delta_3 \left[\mathbf{P}_1 + \mathbf{P}_2 - \mathbf{P}_3 - \mathbf{P}_4 \right] \cdot$$

$$\left[f_3 f_4 \left[1 - f_1 \right] \left[1 - f_2 \right] - f_1 f_2 \left[1 - f_3 \right] \left[1 - f_4 \right] \right] \tag{4.1}$$

for the time evolution of the phase-space density $f_1 = f_1(\mathbf{r}_1, \mathbf{p}_1, t)$.

In this equation v_{12} is the relative velocity of the two incoming nucleons in a N-N collision while $d\sigma/d\Omega$ denotes the in-medium N-N cross section and U is the mean-field potential. In

principle one has to derive U and $d\sigma/d\Omega$ from the same G-matrix. In the present calculation we use $d\sigma/d\Omega = \sigma^{tot}/4\pi$ for the nucleon-nucleon cross section with σ^{tot} determined from σ and ω exchange (M2Y G-matrix) via the optical theorem. This yields an energy dependent nucleon-nucleon cross section which is very close to the values used in cascade simulations[34] but as a function of the nucleon-nucleon c.m. energy lowered by about 15 % to 50 % (Fig. 4). The latter fact is not surprizing since the M2Y potential represents a fit to a G-matrix which includes virtual in-medium interactions and Pauli blocking for intermediate states which results in a reduction of the free nucleon-nucleon interaction. In addition the Pauli blocking for the final states is taken into account via the factor $(1-f(r_i, p_i; t))$ in the collision term.

Independently, the mean field potential U is obtained from a density dependent Skyrme-parametrization,

$$U(\rho(\mathbf{r})) = A \frac{\rho(\mathbf{r})}{\rho_0} + B \left[\frac{\rho(\mathbf{r})}{\rho_0}\right]^\tau , \qquad (4.2)$$

where the three coefficients A, B, and τ are determined by demanding saturation at normal nuclear matter density, the right nuclear matter binding energy, and a certain nuclear compressibility. We choose:

$$A = -218 \text{ MeV}, \quad B = 164 \text{ MeV}, \quad \tau = 4/3 \qquad . \qquad (4.3)$$

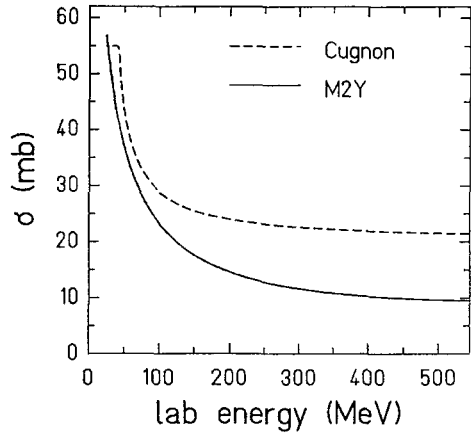The corresponding equation of state in the one-body limit is:

$$\frac{E_B}{A} = \frac{3}{5} \epsilon_0 \left[\frac{\rho}{\rho_0}\right]^{2/3} - 109 \text{ MeV} \frac{\rho}{\rho_0} + 70.3 \text{ MeV} \left[\frac{\rho}{\rho_0}\right]^{4/3} \quad (4.4)$$

where $\epsilon_0 = 38.5$ MeV is the fermi energy. It yields a nuclear matter binding energy of -15.75 MeV, saturates at $\rho_0 = 0.17$ fm^{-3} and results in a nuclear compressibility of K = 235 MeV. We note that when using alternative descriptions for $U(\rho(\mathbf{r}))$ the double differential photon yield is not changed within the numerical uncertainty.

Due to the relatively small contribution of the process $pn \rightarrow pn\gamma$ to the total nucleon-nucleon cross section, it is possible to calculate the photon production perturbatively. In this way we do not couple the emission of the photon back to the nucleonic motion.

We obtain the number of emitted photons N(b) as a function of the impact parameter b by summing (integrating) the differential photon emission probability $d^2\sigma/dE'd\Omega'/\sigma^{tot}$ (cf. Section 3) over all proton-neutron collisions and taking Pauli blocking in the final state phase space of the two nucleons into account:

Fig. 4: The energy dependence of the in-medium nucleon-nucleon cross section as derived from σ- and ω-exchange from the imaginary part of the scattering amplitude in forward direction (full line). The 'free' cross section used in cascade-codes[34] is indicated by the dashed line.

(graph: σ (mb) vs lab energy (MeV), curves labeled Cugnon (dashed) and M2Y (solid))

$$\frac{d^2N(b)}{dE_\gamma d\Omega_\gamma} = \sum_{pn\ coll} \int \frac{d\Omega}{4\pi} \frac{E_\gamma}{E'_\gamma} \frac{d^2\sigma_\gamma}{dE'_\gamma d\Omega'_\gamma} /\sigma^{tot}$$
$$\times \left[1-f(\mathbf{r},\mathbf{p}_3 t)\right] \cdot \left[1-f(\mathbf{r},\mathbf{p}_4,t)\right] . \qquad (4.5)$$

In this equation $\mathbf{r}$ and t indicate the space-time coordinates of each collision. The primes denote quantities in the individual np cm system which have to be transformed into the laboratory frame or the midrapidity frame, respectively. Ω finally denotes the solid angle of the relative momentum $\mathbf{p}_3-\mathbf{p}_4$ which is not fixed by energy and momentum conservation and is chosen here randomly. The integration over $d\Omega/4\pi$ is then performed by an average over many such choices.

To obtain the double differential photon cross section for the nucleus-nucleus reaction, we finally have to integrate over impact parameter:

$$\frac{d^2\sigma}{dE_\gamma d\Omega_\gamma} = \int d^2b \frac{d^2N(b)}{dE_\gamma d\Omega_\gamma} \qquad (4.6)$$

The yields obtained from equation (4.6) can be directly compared to inclusive experimental data without introducing adjustable parameters. We note that in case of pion production by nucleon-nucleon collisions we only have to replace $E/E'd^2\sigma/dE'd\Omega'$ by the corresponding double differential pion cross section and sum over all nucleon-nucleon collisions including pp and nn (cf. Sect. 7).

5. COMPARISON WITH EXPERIMENT

First we compare our results to proton-nucleus data. In the case of a proton-nucleus reaction the incoming proton has fixed momentum given by the beam energy. The neutron has a momentum

distribution and a spatial distribution given by the ground state
configuration of the nucleus. Since the momentum distribution of
the nucleons will not get distorted very much during the course of
the proton-nucleus reaction, the proton-nucleus data serve as a
useful check of the validity of the elementary photon production
cross section.

5.1 Proton-nucleus collisions

In Fig. 5 we compare the results of our calculation for 140 MeV
proton-nucleus collisions to the data of Edgington and Rose[35] for
deuterium, aluminum, and carbon targets. The solid lines represent
the results of a calculation using the relativistic elementary
cross section while the dashed lines show the results for the
semiclassical one (3.1). For the case of deuterium we assumed a
broad spatial distribution of neutrons according to the experi-
mental radius of the deuterium.

Fig. 5: Photon cross section $d\sigma/dE$
for the reaction 140 MeV proton +
nucleus. The solid lines are the
results of our calculation with the
relativistic elementary cross sec-
tion and the dashed lines with the
semiclassical elementary cross sec-
tion. The data are taken from Ref.[35].
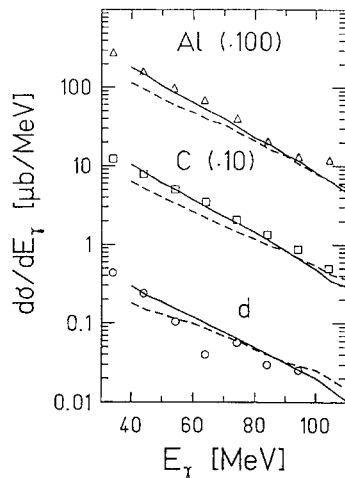
The results of our calculation using the relativistic
elementary cross section show excellent agreement with the
experimental data for p + C and p + Al, while the spectra obtained
with the semiclassical elementary cross section are slightly
flatter than the experimental ones. Therefore, the relativistic
correction of the elementary production cross section, which
becomes more important near the threshold of the high energy
photons, is necessary to explain the high energy photon spectra.

This can be seen more clearly in the angular distribution of
energetic photons. In Fig. 6 we, therefore, plot the differential
cross section for photons with an energy above 40 MeV in the
laboratory system for 140 MeV p + ^{12}C. This figure clearly shows

that the relativistic correction of the elementary photon production cross section is essential to reproduce the angular distribution of energetic photons[35]. We conclude that the microcopic elementary cross section is sufficiently accurate to describe the photon production from incoherent proton-neutron collisions in the nuclear medium.
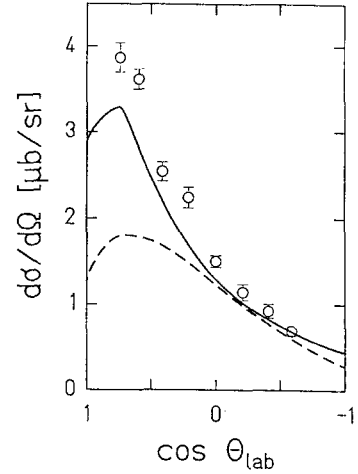
Fig. 6: Comparison of our calcu-
lation to photon angular distri-
butions for the reaction 140 MeV
p + ^{12}C (solid line: relativistic
elementary cross section; dashed
line: semiclassical expression).
The data are taken from Ref.[35].

5.2 Nucleus-nucleus collisions

We compare the results of our calculation within VUU dynamics to experimental data measured by Grosse et al.[1] and Stevenson et al[3]. In Fig. 7 we show the double differential cross section for photons emitted at an angle $\theta = 90°$ with respect to the beam axis.
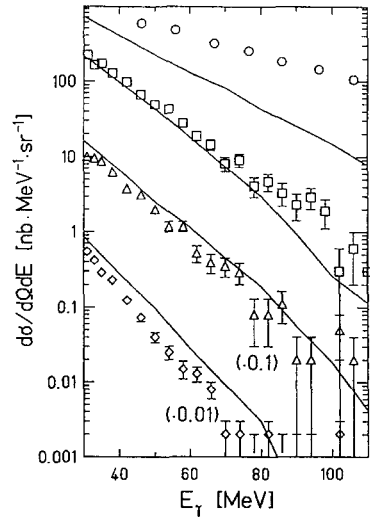
Fig. 7: Photon energy spectra from
heavy-ion collisions. The solid
lines are the results of our calcu-
lations. The symbols represent the
experimental data taken from Ref[1]
and Ref[3]. The emission angle of the
photon is always 90° with respect
to the beam axis. Circles: 84 MeV/u
^{12}C+^{12}C; squares: 40 MeV/u ^{14}N+^{12}C;
triangles: 30 MeV/u ^{14}N+^{12}C;
diamonds: 20 MeV/u ^{14}N+^{12}C.

The three lower curves represent the results from N + C collisions at 40 (squares), 30 (triangles), and 20 (diamonds) MeV/nucleon beam energy[3]. The upper curve shows the results of a $^{12}C+^{12}C$ collision at 84 MeV/nucleon beam energy (circles)[1]. Our calculations with the relativistic elementary cross section (solid lines) are in good agreement with the N+C data from Stevenson et al. with respect to absolute magnitude, spectral slope as well as beam energy dependence. On the other hand, we underpredict the 84 MeV/u C+C data of Grosse et al.[1] by a factor 2.5 to 3.5 indicating that both data might not be compatible with each other. Furthermore, we find the calculated angular distribution to agree well with the data of Stevenson et al., too[36].

5.3 Scaling behaviour of energetic photon yields

In order to get a closer idea of the scaling behaviour in our present treatment we have calculated the inclusive yield of energetic photons for collisions of symmetric systems ranging from mass 12 to mass 70 for a lab. energy of 40 MeV/u. The shape of the spectra as well as the photon angular distribution are found not to change within the numerical uncertainties as a function of mass number. When performing cuts at different photon energies from 50 MeV to 100 MeV and dividing by the respective yield for $^{12}C+^{12}C$ at the same energy we obtain a range of values for fixed mass which is shown in terms of the vertical lines in Fig. 8. The result is compatible with $(A_1 \cdot A_2)^x$ with x = 0.92 which is indicated by the straight line in the double logarithmic plot.

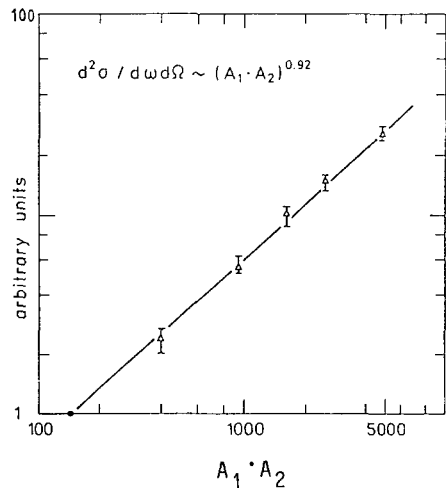Performing a similar analysis for the experimental data from

Fig. 8: Scaling behavior of energetic photon yields with mass number of projectile and target $(A_1 \cdot A_2)$ for nucleus-nucleus collisions at 40 MeV/u. The straight line represents a fit to the calculated values as described in the text. The vertical bars give the cross section for various γ-energies between 50 and 100 MeV.

$$d^2\sigma \: / \: d\omega d\Omega \sim (A_1 \cdot A_2)^{0.92}$$

arbitrary units

$A_1 \cdot A_2$

Ref.[8] we obtain x = 0.87 ± 0.05 well in line with our calculations. One should note that contributions from collective bremsstrahlung, which might not be neglected for very heavy systems[17], would yield a higher value of x in the region of heavy nuclei than for light nuclei. Experimental data, however, show a slightly decreasing scaling exponent[8] for heavy systems.

6. PHASE-SPACE ANALYSIS OF ENERGETIC PHOTON PRODUCTION

In this Section we are now interested in the dynamical origin of energetic photons in momentum and coordinate space. We consider a schematic np collision in momentum space producing a photon with momentum $\mathbf{k}$ and energy $E = \hbar ck$. The momenta of the colliding nucleons further on are denoted by $\mathbf{k}_1$ and $\mathbf{k}_2$, respectively, while their final momenta $\mathbf{k}_3$ and $\mathbf{k}_4$ are determined by momentum and energy conservation (cf. Section 4). A photon with energy E is then produced in the angular range $d\Omega$ (with respect to the np c.m.s. and np axis) with the elementary probability $d^2\sigma/dEd\Omega/\sigma^{tot}$ where σ^{tot} denotes the total angle integrated nucleon-nucleon cross section for a relative momentum $|\mathbf{k}_1-\mathbf{k}_2|$, multiplied by the probability that the phase-space cells around $\mathbf{k}_3$ and $\mathbf{k}_4$ are not occupied. Thus the relative probability for γ-production in the pn collision i in a fixed frame of reference, taking place at $t = t_i$ and $\mathbf{r} = \mathbf{r}_i$, is given by

$$W_i(\mathbf{k}_1,\mathbf{k}_2;\mathbf{k}) = 1/\sigma^{tot}(|\mathbf{k}_1-\mathbf{k}_2|)\ \frac{E}{E'}\ \frac{d^2\sigma}{dE'd\Omega'}$$
$$\times\ \left[1-f(\mathbf{r}_i,\mathbf{k}_3;t_i)\right]\left[1-f(\mathbf{r}_i,\mathbf{k}_4;t_i)\right],\qquad (6.1)$$

where the phase-space distribution is evaluated from VUU dynamics (cf. Section 4). Here γ-energy and γ-angle are properly Lorentz-transformed from the nucleon-nucleon c.m. system to the laboratory frame.

The first question we address is related to the area in momentum space which contributes to the production of a photon with energy $E = 100$ MeV under $90°$ in the laboratory frame with respect to the beam (z-) axis. The answer to this question can be obtained by summing W_i over all np collisions

$$R(\mathbf{k}_1) = \sum_i \sum_{\mathbf{k}_2}\ W_i(\mathbf{k}_1,\mathbf{k}_2;\mathbf{k}_\gamma) \qquad\qquad (6.2)$$

where we integrate also over $\mathbf{k}_2$ in order to reduce the number of degrees of freedom in $R(\mathbf{k}_1)$. Since $\mathbf{k}_1$ and $\mathbf{k}_2$ can be exchanged no information is lost in this integration.
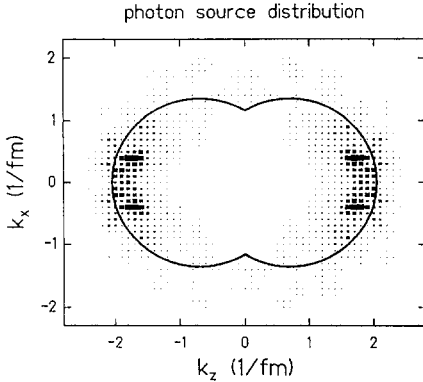
photon source distribution

occupation factor $(1-f(k_x,k_y=0,k_z))$

Fig. 9: The distribution of nucleons $R(\mathbf{k})$ (6.2) in momentum space which produce a 100 MeV photon at 90° in a central collision of $^{12}C+^{12}C$ at 40 MeV/u. The momentum distribution corresponding to the infinite nuclear matter limit is given in terms of the shifted Fermi spheres.
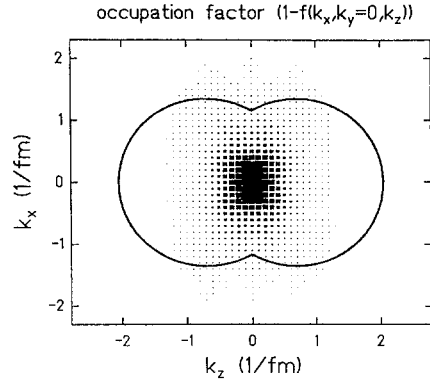
Fig. 10: The final phase-space probability $P(\mathbf{k})$ (6.3) for final states of nucleons producing a 100 MeV photon at 90° in a mutual collision for $^{12}C+^{12}C$ at 40 MeV per nucleon.

The result for $R(\mathbf{k}_1)$ is shown in Fig. 9 in terms of a cluster plot for a central collision of $^{12}C + ^{12}C$ at 40 MeV/u. We also display the phase-space distribution in the infinite nuclear matter limit given by two nonintersecting Fermi spheres shifted by ≈ 1.4 fm^{-1} in beam direction according to the bombarding energy. It is clearly seen that a 100 MeV photon is dominantly produced by nucleons which come from the endcaps in z-direction of the elongated momentum distribution. Due to successive nucleon-nucleon collisions these energetic nucleons are available only in the initial phase of the heavy-ion reaction.

The second question addresses the fate of nucleons after producing a 100 MeV γ-ray. Due to energy and momentum conservation the region with $\mathbf{k} \approx 0$ is favored, but it is Pauli-forbidden in the infinite nuclear matter limit. To see the actual population of this region we show the probability that the phase-space around $\mathbf{k}_3$ is vacant:

$$P(\mathbf{k}_3) = \sum_i \left[1-f(\mathbf{r}_i;\mathbf{k}_3;t_i)\right] \qquad (6.3)$$

in Fig. 10. Here we have summed over all pn collisions i that produce a 100 MeV photon at 90° (for $^{12}C+^{12}C$ at 40 MeV/u). $\mathbf{k}_3$ and $\mathbf{k}_4$ are constrained by momentum and energy conservation while the remaining relative angle Ω is chosen randomly and then averaged out. The shifted Fermi spheres corresponding to the infinite

nuclear matter limit are also displayed in Fig. 10 for ease of comparison.

We find that the $\mathbf{k} \approx 0$ region is indeed strongly favored. That there is any free phase-space in this region in contrast to the infinite nuclear matter limit can be traced back to distortions in phase space for finite colliding nuclei which keep the low momentum region around $\mathbf{k} \approx 0$ unoccupied[15,17,37]. Nucleon-nucleon collisions start to fill up this part of phase space within roughly 10 to 15 fm/c[37] so that this effect again limits the production of energetic γ-rays to the early phase of the heavy-ion collision.

The apparent source-velocity distribution of high energy photons in the laboratory frame is found to be approximately symmetric in the nucleon-nucleon c.m.s. from our calculations for symmetric and asymmetric systems[36] indicating that the dominant yield of photons arizes from first pn collisions.

The latter conclusion is supported by the photon source distribution in coordinate space which is plotted in Fig. 11 for a central collision of $^{12}C+^{40}Ca$ at 40 MeV/u in the laboratory frame for photons with energy E = 50 MeV emitted perpendicular to the beam (z-direction). The position of ^{40}Ca in the lab. system is indicated by the full circle while the ^{12}C nucleus is impinging from the left. The photon source distribution is essentially localized within the initial overlap regime of the colliding nuclei indicating again photon production in the early phase of the reaction.

target photon source distribution

Fig. 11: The photon source distribution in coordinate space for a central collision of $^{12}C+^{40}Ca$ at 40 MeV/u in the laboratory frame for photons with energy E = 50 MeV emitted perpendicular to the beam axis. The position of ^{40}Ca at rest in the lab. system is indicated by the full circle while the ^{12}C nucleus is impinging from the left.
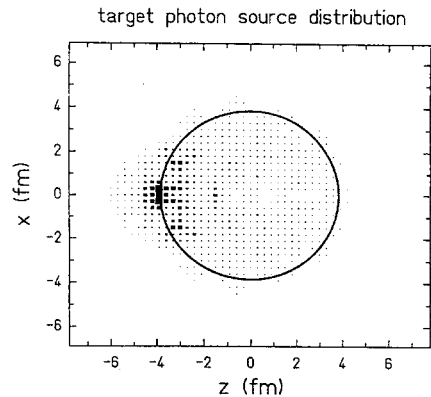
## 7. PION PRODUCTION BY INCOHERENT NUCLEON-NUCLEON COLLISIONS

The apparent success of the present incoherent nucleon-nucleon model with respect to high energy γ-ray production promises interesting perspectives for subthreshold pion production by two-

body mechanism, too. Indeed, there is a rather long history
concerning pion production by nucleon-nucleon collisions in the
overlap regime of colliding nuclei dating back to Mc Millan and
Teller in 1947[38] and a couple of stationary and dynamical two-
nucleon approaches have been performed [37-46]. Apart from the
quantal phase-space model of Ref.[37] no satisfactory results for
bombarding energies below 60 MeV/u have been obtained so far and it
appears worth looking at the problem within the present dynamical
approach. As indicated in Section 4 the production probability in
(4.5) $E_\gamma/E_\gamma' \ d^2\sigma_\gamma/dE_\gamma' d\Omega_\gamma'/\sigma^{tot}$ has to be replaced by $d^2\sigma_\pi/dE_\pi d\Omega_\pi/\sigma^{tot}$
when neglecting the transformation from the individual nucleon-
nucleon cms to the midrapidity frame which due to kinematics
roughly coincide (cf. Fig. 9 in case of energetic photons). The
elementary production cross section can again be evaluated from
various Feynman diagrams[46], however, including explicitly the
Δ-degree of freedom. In our present investigation we proceed in a
different way and adopt the experimental values for the free
production process from Ver West and Arndt[47] as in Ref.[37] and
assume σ^{tot} to be given by the free nucleon-nucleon cross section
averaged over isospin, too.

Since experimental pion spectra[48-56] show exponential distri-
butions of slope E_0^{-1} depending only on the relative velocity of the
colliding ions and not on the projectile/target system we assume
the average pion energy to be given by E_0 and adopt E_0 from Ref.[1]
as a function of bombarding energy. The pion direction is chosen
randomly by Monte Carlo and for each individual nucleon-nucleon
collision the final nucleon momenta are determined by energy and
momentum conservation. A remaining relative angle Ω'', which is not
determined by the kinematical constraints, is averaged out by Monte
Carlo again. An integral over impact parameter (cf. (4.6)) gives
the inclusive pion yield for all systems and laboratory energies
desired.

The inclusive neutral pion yield expected from individual
nucleon-nucleon collisions for $^{40}Ca+^{40}Ca$ is shown in Fig. 12 by the
full line as a function of the laboratory energy per nucleon in
comparison with experimental data from Refs.[48-56] scaled by
$(A_1 \cdot A_2)^{.68}$ to the system $^{40}Ca+^{40}Ca$. We overestimate the data by
roughly a factor of 2 at all energies down to 30 MeV/u which might
indicate either pion absorption in the nuclear medium or a
reduction of the NΔ cross-section in the medium[57]. When adopting a

Fig. 12: Inclusive neutral pion yield for $^{40}Ca+^{40}Ca$ as emerging from individual nucleon-nucleon collisions as a function of bombarding energy (full line) in comparison with experimental data from Refs.[48-56] scaled by $(A_1 \cdot A_2)^{.68}$. The dashed line is obtained when including pion reabsorption with $\lambda = 5$ fm.

total pion yield
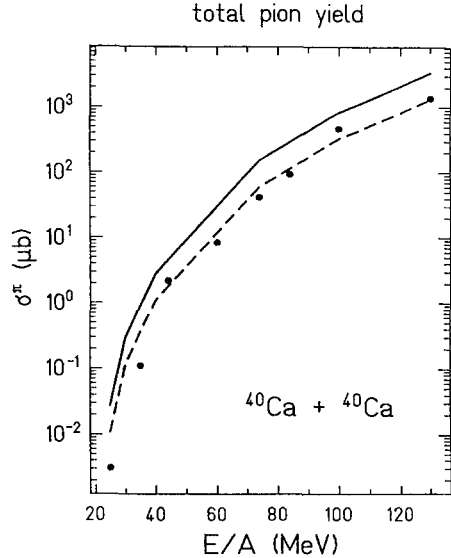
pion mean-free-path $\lambda \approx 5$ fm we obtain the dashed line in Fig. 12 which roughly coincides with the experimental data over 4 orders of magnitude in cross section leaving minor room for cooperative phenomena. We note that a similar analysis as in Section 5.3 for the scaling law of the inclusive cross section yields

$$\sigma_{\pi^0} \sim (A_1 \cdot A_2)^X \qquad\qquad (7.1)$$

with $x = 0.87$ for $\lambda = \infty$ and $x = 0.73$ for $\lambda = 5$ fm[58]. The observed subthreshold pion yield thus appears also to be consistent with the picture of production by independent nucleon-nucleon collisions in the early phase of the heavy-ion reaction.

8. CONCLUSION

We have performed a microscopic study of energetic photon production in proton and heavy-ion induced reactions based on a covariant model for bremsstrahlung from elementary proton-neutron collisions. Our detailed dynamical investigations allow for the following conclusions:

i)   the yield of high energy γ-rays from collective bremsstrahlung is down by roughly an order of magnitude as compared to experimental data;

ii) energetic photon production is limited to the early stage of the reaction and dominated by first chance proton-neutron collisions;

iii) the apparent source velocity is associated with the nucleon-nucleon frame of reference, i.e. the midrapidity domain;

iv) since proton-nucleus and nucleus-nucleus collisions are described on the same footing our simultaneous reproduction of both sets of experimental data leaves only minor room for coherent and cooperative reaction mechanisms (cf.i));

v) the high yield of photons observed must be attributed to distortions in phase-space which keep the midrapidity regime partly unblocked during the initial phase of the reaction;

vi) inclusive yields of energetic photons roughly scale with $(A_1 \cdot A_2)^{.92}$.

Apart from the problem of pion reabsorption in the nuclear medium inclusive pion yields are found to be well in line with the expectation of being produced by individual nucleon-nucleon collisions in the early phase of the heavy-ion reaction in close analogy to energetic photons. Exclusive experiments, however, are needed for more accurate tests of the present theory.

ACKNOWLEDGEMENTS

REFERENCES

1) E. Grosse et al: Europhys. Lett. 2 (1986) 9
2) N. Herrmann et al: GSI Annual Report 1985, p. 86
3) J. Stevenson et al: Phys. Rev. Lett. 57 (1986) 555
4) M. Kwato Njock et al: Phys. Lett. 175B (1986) 125
   R. Bertholet et al: submitted to Nucl. Phys. A
5) K. Beard et al: Phys. Rev. C32 (1986) 1111
6) N. Alamanos et al: Phys. Lett. 173B (1986) 392
7) R. Hingmann et al: Phys. Rev. Lett. 58 (1987) 759
8) P. Grimm, PhD Thesis, GSI Report 87-2
9) D. Vasak et al: Nucl. Phys. A428 (1984) 291c
   J. Phys. G11 (1985) 1309
10) D. Vasak: Phys. Lett. 176B (1986) 276
11) T. Stahl et al: Z. Phys. A327 (1987) 311
12) R. Shyam and J. Knoll: Nucl. Phys. A448 (1986) 322
13) H. Nifenecker and J.P. Bondorf: Nucl. Phys. A442 (1985) 478
14) C.M. Ko et al: Phys. Rev. C31 (1985) 2324
15) W. Cassing et al: Phys. Lett. 181B (1986) 217
16) M. Tohyama, Phys. Lett. 144B (1984) 169;
    Nucl. Phys. A437 (1985) 443
17) W. Bauer et al: Phys. Rev. C34 (1986) 2127
18) J.D. Jackson; Classical electrodynamics (Wiley, New York, 1962), chapter 15
19) D. Neuhauser and S.E. Koonin; Nucl. Phys. A462 (1987) 163

20) R. Baier et al: Nucl. Phys. B11 (1969) 675
21) G.E. Bohannon et al: Phys. Rev. C16 (1977) 284
22) V.R. Brown and J. Franklin; Phys. Rev. C8 (1973) 1706
23) P.F.M. Koehler et al: Phys. Rev. Lett. 18 (1967) 933
24) G.F. Bertsch et al: Phys. Rev. C29 (1984) 673
25) H. Kruse et al: Phys. Rev. Lett. 54 (1985) 289;
     Phys. Rev. C31 (1985) 1770
26) J. Aichelin and G.F. Bertsch; Phys. Rev. C31 (1985) 1730
27) W. Gordon, Z. Phys. 50 (1930) 630
28) W. Bauer et al: Nucl. Phys. A456 (1986) 159
29) R.Y. Cusson et al: Phys. Rev. Lett. 36 (1976) 1166;
     Phys. Rev. C18 (1978) 2589; Phys. Rev. Lett. 42 (1979) 694
30) J.D. Walecka: Ann. Phys. (NY) 83 (1974) 491
31) K. Chen et al: Phys. Rev. 166 (1968) 949
32) G.F. Bertsch et al: Nucl. Phys. A284 (1977) 399
33) C. Itzykson, J.-B. Zuber:
     Quantum Field Theory, Mc Graw-Hill, 1985, p. 697
34) J. Cugnon et al: Nucl. Phys. A352 (1981) 505
35) J.A. Edgington and B. Rose: Nucl. Phys. 89 (1966) 523
36) T.S. Biro, K. Niita, A.L. De Paoli, W. Bauer, W. Cassing,
     U. Mosel; Nucl. Phys. A, submitted
37) W. Cassing: Phase Space Approach to Nuclear Dynamics, ed. by
     M. Di Toro, World Scientific Publ. Comp.; Singapore 1986, pp.
     64-93
38) W.G. McMillan and E. Teller: Phys. Rev. 72 (1947) 1
39) G.F. Bertsch: Phys. Rev. C15 (1977) 713
40) B. Jakobsson et al: Phys. Lett. 82B (1979) 35
41) B. Jakobsson: Phys. Scripta T5 (1983) 207
42) C. Guet and M. Prakash: Nucl. Phys. A428 (1984) 119c
43) M. Tohyama, R. Kaps, D. Masak, and U. Mosel:
     Phys. Lett. 136B (1984) 226; Nucl. Phys. A437 (1985) 739
44) J. Aichelin: Phys. Lett. 164B (1985) 261
45) M. Blann: Phys. Rev. C32 (1985) 1231
46) R. Kaps et al: Z. Phys. A326 (1987) 97
47) B.J. Ver West and R.A. Arndt: Phys. Rev. C25 (1982) 1979
48) W. Benenson et al: Phys. Rev. Lett. 43 (1979) 683
49) T. Johansson et al: Phys. Rev. Lett. 48 (1982) 732
50) S. Nagamiga et al: Phys. Rev. Lett. 48 (1982) 1780
51) H. Heckwolf et al: Z. Phys. A315 (1984) 243
52) H. Noll et al: Phys. Rev. Lett. 52 (1984) 1284
53) P. Braun-Munzinger et al: Phys. Rev. Lett. 52 (1984) 255
54) E. Chiavassa et al: Nucl. Phys. A422 (1984) 621
55) J. Stachel et al: Phys. Rev. C33 (1986) 1420
56) E. Grosse: Nucl. Phys. A447 (1985) 611c
57) B. ter Haar and R. Malfliet: Preprint KVI-651
58) A.L. De Paoli, K. Niita, T.S. Biro, W. Bauer, W. Cassing, and
     U. Mosel: Preprint UGI-87-15